On the H_2 Interaction on Transition Metal Adatoms Supported on Graphene: A Systematic Density Functional Study

Montserrat Manadé [a], Francesc Viñes [a], Adrià Gil [b,c,*], and Francesc Illas[a,*]

[a] *Departament de Ciència de Materials i Química Física & Institut de Química Teòrica i Computacional (IQTCUB), Universitat de Barcelona, c/Martí i Franquès 1,08028 Barcelona, Spain.*
[b] *Centro de Química e Bioquímica, DQB, Faculdade de Ciências, Universidade de Lisboa, Campo Grande 1749-016 Lisboa, Portugal.*
[c] *CIC Nanogune, Tolosa Hiribidea 76, 20018 San Sebastian, Spain.*

Abstract

The attachment of H_2 to the *full* set of Transition Metal (*TM*) adatoms supported on graphene is studied here by density functional theory. Methodology validation calculations on the interaction of H_2 to benzene and graphene show that any of the vdW corrections under study, Grimme D2, D3, D3BJ, and Tatchenko-Scheffler, applied on PBE functional, are similarly accurate to describe such subtle interactions, with an accuracy of almost 2 kJ mol^{-1} compared to experiments. PBE-D3 results show that H_2 physisorbs on specially stable d^5 or d^{10} TMs. In other 5*d* metals, and rightmost 3*d* and 4*d* ones, H_2 dissociates, and only for Y, Mn, Fe, and Zr the H_2 binds strong enough for its storage in the so-called Kubas mode, where H_2 bond is sensibly elongated. Other metals (Co, Ni, Ru, Rh, Pd) feature also an elongated Kubas mode, interesting as well for H_2 storage. Sc and Ti also display a Kubas mode, especially suited given their lightness for meeting the gravimetric requirements. The H_2 interaction with TM adatoms implies a TM→H_2 charge transfer, while the magnetic moment of the system tends to remain intact, except for early 5*d* TMs, where the unpaired electron transfer seems to be associated to the H_2 bond breakage.

*Corresponding Authors: Tel: 00 34 93 402 1129; E-mail: francesc.illas@ub.edu (Francesc Illas) and Tel: 00 351 217 500 845; E-mail: agmestres@fc.ul.pt (Adrià Gil).

1. Introduction

Hydrogen (H_2) based energy technologies are currently investigated as the best substitute to fossil fuels for a future clean, renewable, and environmentally friendly energy economy, while meeting at the same time the worldwide growing energy demands. The harmless generation of water (H_2O) upon H_2 combustion, together with an easy H_2 gas stream formation from hydrocarbon reforming, the water gas shift reaction, or even *via* H_2O splitting by electrolysis or photocatalysis, are appealing aspects which go for its usage. However, H_2 economy is impeded hitherto by the absence of a secure yet economically suitable way for its on-board storage. The Department of Energy (*DOE*) of the United States of America (*USA*) settled the material properties needed for H_2 storage: It must *i)* have a gravimetric storage capacity above 5.5 weight percentage (wt%) within -40 ºC (tundra) and 60 ºC (desert) temperatures,[1] while *ii)* displaying structural stability during repeated hydrogen storage cycles, a *iii)* rapid gas uptake at a charging pressure of *ca.* 30 bar, alongside a fast release at a discharging pressure of around 1.5 bar,[2] and, finally, *iv)* cost-effectiveness for its implementation. A critical aspect seems to be the attachment strength of H_2 to the employed material. The H_2 adsorption energy should range 0.16-0.26 eV per adsorbed H_2 molecule — 15.44-25.08 kJ mol^{-1}— for an optimal fast uptake and release,[2,3] yet larger values up to 0.6 eV —57.89 kJ mol^{-1}— can be useful.

In order to meet the gravimetric requirement light materials with high surface area have been explored, being Carbon-based materials a natural sandbox to play with.[4] However, weak adsorption on activated carbon and graphite allows storage only at cryogenic temperatures, and, despite intercalation within graphite allows for larger storage, its release is impeded.[4] Graphene and carbon nanotubes (*CNTs*) were considered as extended systems to store H_2 onto, even combined in pillared graphene,[5] although Density Functional (*DF*) calculations revealed a weak interaction with H_2 ranging 1.05-1.38 kJ mol^{-1}, and so, only

feasible at very low temperatures. This goes along with detailed DF studies on the adsorption of H_2 on CNTs and graphene, where low adsorption energies of 6.56 and 8.30 kJ mol^{-1} were obtained, respectively,[6,7] even when gained at the Local Density Approximation (*LDA*) level, known to overestimate the interatomic interactions. In the case of carbon cluster structures, LDA estimates are of 6.75 kJ mol^{-1}, and so, too weak as well.[8]

Far from discourage, further and present research is addressed at enhancing the H_2 attachment to such carbon-based structures. In that sense, analogous boron nitride nanotubes and sheets have been explored,[9,10] with adsorption energies not exceeding 1.25 kJ mol^{-1} according to DF calculations within the Generalized Gradient Approximation (*GGA*), yet inclusion of van der Waals (*vdW*) forces may rise this value up to 14.47 kJ mol^{-1} in *h*-BN sheets.[9] Another strategy to enhance the H_2 physisorption to adequate levels is to functionalize the carbon or BN based structures, mostly with light alkaline or alkaline earth metals, where Li, Be, and Ca are probably exemplary cases.[5,8,11-15] The idea is to use such metal atom centres, typically positively charged (cations), as anchor points for H_2, which would adsorb H_2 in the so-called Kubas mode;[16,17] a η^2 coordination mode where H_2 bond length is elongated by ~0.06-0.16 Å. This mode displays adsorption energies on such cations ranging 0.2-0.4 eV —19.30-38.59 kJ mol^{-1}—, as obtained at LDA level,[8,12,15] and therefore, interesting for practical applications. However, these atomic cations feature low adsorption energies, below the parent metal bulk cohesive energy. Compare, for instance, the GGA adsorption energy of Li on graphene of 0.22 eV[18] as obtained using the Perdew-Burke-Ernzerhof (*PBE*)[19] exchange-correlation (*xc*) functional, to the experimental cohesive energy of bulk Li of 1.66 eV.[20] This adds up with low energy barriers for the metal diffusion, calculated to be of 0.28 eV at PBE level,[18] which suggests that Li would easily diffuse and aggregate to form metallic Lithium, eventually losing its H_2 anchoring properties by a lower interaction towards H_2 and a reduced exposed surface area. Nevertheless, a high attachment

energy of Li onto carbon fullerenes apparently prevent its clusterization, and DF studies using the Perdew-Wang 91 (PW91) GGA functional[21] yielded adsorption energies of up to 0.18 eV —17.37 kJ mol^{-1}—.[22]

In any case, the idea of displaying isolated metal adatoms opened the path to explore other systems, such as light Transition Metals (*TMs*) Sc, Ti, and V on C_{60} buckyballs[23-25] or CNTs,[26,27] with promising adsorption energies ranging 0.2-0.6 eV—19.30-57.89 kJ mol^{-1}— as obtained at GGA level, and a foreseen load up to 8-9 wt%.[23,26] However, the TMs adsorption energy is below the bulk cohesive energy, and that, together with low diffusion energies, would lead to a clustering and loss of the metal exposed surface area, ultimately decimating the adsorption wt%,[25] although, apparently, an energetic toll has to be paid for this process to occur.[22] However, as extracted from our previous DF works including vdW, some TMs can strongly attach on graphene and CNTs while displaying diffusion energy barriers above 0.3 eV, thus allowing for a survival of TMs in a single-atom fashion.[28,29] Indeed, a recent study on most of 3*d* TMs highlights the suitability of Sc, Ti, Co, and Fe as possible anchor points for hydrogen storage,[30] whereas another study contemplated the case of late transition metal Pt.[31] The diffusion energy barriers were experimentally confirmed on Ti, Fe, and Ni,[32] where a continuous coverage was observed for Ti and Fe on CNTs, and nanosized particles for Ni. Even so, there exist strategies to prevent clusterization, including N or B doping,[33] or by introducing carbon defective sites, such as vacancies,[34] and steps.[35] These strategies increase the binding energy of TMs to be higher than the bulk cohesive energy and/or increase the adatom diffusion energy barriers so as to kinetically avoid clusterization. The profiting of such strategies is nowadays a matter of intense research not only concerning H_2 economy,[34-37] but also for single transition adatom stabilization and usage as singe-atom catalysts for heterogeneously catalysed uses.[38,39]

Nevertheless, most H_2 studies mainly focus on the maximum capacity for hydrogen storage on considered substrates and, as far as we know, no systematic studies have been found in the literature analyzing how the first adsorbed H_2 interacts with the full set of TM functionalizing graphene, thus giving information of the interaction along the row and down the group by using DFT methods including corrections to vdW forces. Aside, exhaustive studies across composite materials are gaining momentum and importance for materials informatics,[40,41] where big data and machine learning machineries can be fully exploited towards materials design and isolation, a field where bright initiatives such as Materials Project and Novel Materials Discovery excel.[42-44]

In particular, the aims of this work are *i*) the calibration of several vdW approaches to be used for the study of the H_2 adsorption on TM functionalized graphene and *ii*) the analysis of the TM functionalized graphene when interacting with the first adsorbed H_2 molecule, taking into account the full set of TMs to see the behavioural trends along rows and groups. Here we provide so by a comprehensive study exploring structural, energetic, and magnetic properties of the first H_2 molecule anchored to the *full* sets of 3*d*, 4*d*, and 5*d* TMs atoms supported on graphene, being a representative carbon structure, although results could well be extrapolated to graphite, CNTs, and fullerenes. The study is carried out at standard DF GGA level, but including a proper description of vdW forces, first tested against highly accurate *golden standard* Coupled Cluster Singles Doubles with perturbative Triples [*CCSD(T)*] results and experimental data. The behavioural trends along the *d* series allow to interpret the preference for dissociative H_2 adsorption, Kubas connection situations, or physisorption to graphene, paving the way for the future study on promising systems for H_2 storage, yet other applications, such as usage of single-atom TM catalysts in hydrogenation reactions, are also envisaged. We expect that this systematic study will give information about which correction

to vdW forces is better for GGA DF methods and will enlighten the understanding of hydrogen interactions on TM functionalized carbon based substrates.

2. Computational Details

Spin polarized DF calculations have been performed using the Vienna *Ab initio* Simulation Package —VASP.[45] The Projector Augmented Wave (*PAW*) method has been used to represent atomic cores effect on the valence electron density.[46] This simulation of the core states allows one to obtain converged results —energy variations below 0.01 kJ mol^{-1}— with a cut-off kinetic energy of 415 eV for the plane-wave basis set. Geometry optimizations were performed using a conjugated gradient algorithm and applying a first-order Methfessel-Paxton smearing of 0.2 eV width, yet final energies were corrected to 0 K (no smearing). The structural optimizations were carried out allowing to relax all atomic degrees of freedom, and were finalized when forces acting on atoms were below 0.01 eV $Å^{-1}$. All DF calculations have been carried out using the PBE xc functional,[19] a representative GGA. This functional has been previously found to essentially match the graphene cell parameter of 2.46 Å,[47] and also to yield the best overall description of TMs among many LDA, GGA, meta-GGA, and hybrid functionals.[48,49]

Energy and structure optimizations have been carried out on a *p*(4×4) graphene slab supercell, used as a representative carbon-based material, since previous studies report a similar qualitative behaviour for graphene and CNTs, as far as TM adsorption and H_2 anchoring to them are concerned.[28,30] The supercell dimension grants a separation between adsorbed TM adatoms of ~1 nm, enough to avoid interactions with TM adatoms on periodically repeated adjacent cells, and so as well for the anchored H_2 molecules.[29] A vacuum region of 1 nm is added in the direction normal to the graphene layer, in order to avoid interactions between repeated graphene sheets. Test calculations with double vacuum

yielded variations in the energy of ~0.003 eV, i.e. 0.30 kJ mol^{-1}, and so this value is taken as our present set up degree of accuracy. An optimal Monkhorst-Pack[50] **Γ**-centred **k**-point grid of 2×2×1 dimensions was used, having a similar **k**-point density as in earlier reports.[47]

Mind that for any TM atom adsorbed on graphene the adsorption energy, E_{ads}^{TM}, is defined as

$$E_{ads}^{TM} = (E_G + E_{TM}) - E_{TM/G} \quad (1),$$

where $E_{TM/G}\mathrm{E}_{\mathrm{slab}}^{\mathrm{fix}}$ is the total energy of graphene layer with the TM adatom attached, $E_G\mathrm{E}_{\mathrm{bulk}}$ is the total energy of the pristine graphene layer, and E_{TM} the total energy of an isolated TM atom as previously[48] or presently calculated by placing the TM isolated in a box of 9×10×11 Å dimensions and carrying out a **Γ** point calculation. Accordingly, the H_2 adsorption energy on a TM adatom, $E_{ads}^{H_2}$, is defined as

$$E_{ads}^{H_2} = (E_{H_2} + E_{TM/G}) - E_{H_2/TM/G} \quad (2),$$

where E_{H_2} is the **Γ**-point energy of the H_2 molecule optimized within the 9×10×11 Å cell, and $E_{H_2/TM/G}$ the energy of the H_2 molecule adsorbed on the TM adatom supported on graphene. According to the employed signs in Eq. 2, adsorption energies are here defined positive, and hence, the larger the E_{ads} value, the stronger the interaction between graphene and the TM atom or between H_2 and the TM@graphene system. The adsorption energies for H_2 adsorbed on benzene are calculated likewise, see below. The TM adsorption by different approaches, see below, yielded small variations of the graphene corrugation of ±0.02 Å when compared to the values obtained before.[29] Furthermore, when H_2 is adsorbed on TM@graphene, the corrugation of graphene reduces by ~0.03 Å at most. Charges on TM adatoms, Q_{TM}, and for the H_2 molecule, Q_{H_2}, have been estimated through a Bader analysis of the electron density.[51] H_2 bond length d(HH) has been measured in each computed case, as well as the average distance between H_2 atoms and the TM adatom, $\bar{d}$(MH). Global magnetic moments have been

acquired for the found stable minima. Notice that in none of the studied cases a finite bandgap was found for graphene, which maintains its semi-metallic character, yet doped in contact with TM adatoms.[29]

Description of the vdW dispersive forces has been accounted *via* the D3 dispersion correction of Grimme,[52] known to be among the best corrections on describing the interaction of H_2 to a variety of inorganic clusters,[53] although a comparison is made to previous calculations using D2 correction,[54] which was found to accurately describe the interaction of TM adatoms on graphene.[29] For the D2 correction, the dispersion coefficients, C_6, and vdW radii, R_0, were collected from the original paper for 3*d* and 4*d* TMs,[52] and those for 5*d* metals were taken from a posterior study.[55] Furthermore, for completeness, Becke-Jonson (*BJ*) damping on D3 (*D3BJ*) correction has also been contemplated,[56] as well as the (*TS*) correction.[57]

For the evaluation of H_2 adsorption on benzene, three different codes were used. On one hand, VASP calculations were carried out by optimizing benzene in a supercell of 20×20×20 Å dimensions at **Γ**-point, and later optimizing H_2 at various positions in close contact to benzene, with the same settings as detailed above. Aside, we employed the *Ab Initio* Simulation Package —AIMS,[58,59] where electron density is described with a basis set of Numeric Atom-centered Orbitals (*NAO*), with light grid Tier-1 basis set options, a basis set quality comparable (or better than) to double-ζ plus polarization Gaussian Type Orbitals (*GTO*) aug-cc-pVDZ basis.[60] Last, we also carried out calculations on molecular models consisting of benzene and H_2 by means of Gaussian09.[61] We used here three dispersion methods; D2, D3, and D3BJ, employing NASA Ames ANO extended basis set to avoid Basis Set Superposition Error (*BSSE*).[62]

3. Results and Discussion

3.1. H_2 Adsorption on Benzene

First of all, in order to properly address the H_2 interaction with TM adatoms supported on graphene, one needs to validate the employed methodology, especially on describing weak vdW interactions. This is a challenging task as far as the interaction of H_2 with graphene is very weak, ranging 4-6 kJ mol^{-1}, similar to the experimental value on CNTs[63] of 5.98 kJ mol^{-1} and the value of 5.00±0.05 kJ mol^{-1} on graphite.[64] So, the accuracy limits are a quite severe threshold. A common practice, when possible, is to use CCSD(T) calculations as a reference —a *golden standard*— to which methods are tested against, a usual strategy employed in the past for H_2 storage.[53,65-67] A previous study tackled the H_2 interaction with benzene (C_6H_6) at CCSD(T) level, showing a H_2 geometry where the molecule is placed perpendicular and over the centre of the benzene ring, see Fig. 1a, with an adsorption energy of 3.06 kJ mol^{-1}.[68] However, in that study only perpendicular H_2 situation was contemplated, based on a topological exploration over fluorobenzene (C_6H_5F), although posterior studies employing the vdW-DF2 functional[69] showed a quasi degeneracy —adsorption energy difference of only 0.05 kJ mol^{-1}— in between the perpendicular interaction, and that of H_2 bond lying parallel to the benzene plane, also with the H_2 molecular gravimetric centre over the benzene ring centre, and with the molecular axis pointing towards benzene C-C bonds, see Fig. 1b.[65] A posterior study at CCSD(T) carried out at the Complete Basis Set (*CBS*) limit delivered an interaction energy of 4.34 and 3.06 kJ mol^{-1} for the perpendicular and parallel conformations, respectively.[66] Note as well that a different orientation can be imposed to parallel H_2; that with the molecular axis pointing towards opposite benzene C atoms, see Fig. 1c.

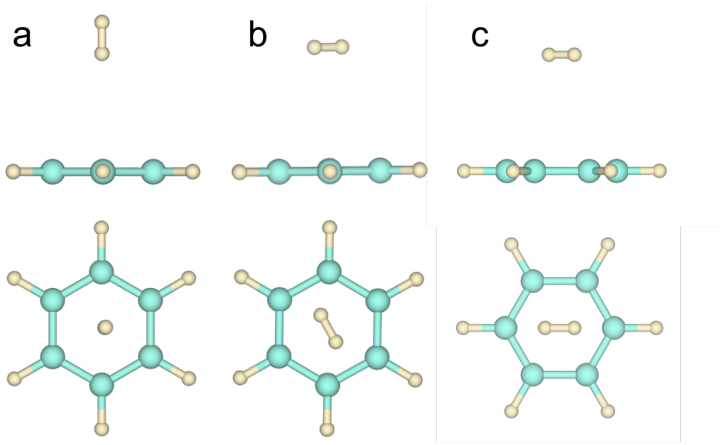

Fig. 1 Top (bottom) and side (top) views for H_2 interacting on benzene on a) perpendicular fashion, Pe, or b) parallel and oriented to C-C bonds, Pa_1, or c) parallel and oriented towards opposite C atoms, Pa_2. Green and yellow spheres denote C and H atoms, respectively.

To get unbiased results, and to explore the possibility of H_2 being adsorbed on a parallel fashion, calculations were carried out for both the perpendicular and planar conformations, at PBE GGA level, together with D2, D3, D3BJ, and TS vdW corrections, with the obtained values encompassed in Table 1, as gained using different codes. Results show that perpendicular adsorption is clearly favourable with respect parallel conformations, displaying interaction energies ~0.9 kJ mol^{-1} or larger than the parallel ones, in agreement with CCSD(T) data.[66] Structurally, the H_2 bond length, *d*(HH), remains essentially unperturbed —variations below 0.001 Å— when interacting with benzene molecule at any computed level. However, the H_2 adsorption height, seized by the distance in between the H_2 and benzene gravimetric centres, *h*, does significantly change depending of the employed method, even basis set. For instance, calculations employing plane waves show how H_2 is placed around 3 Å above benzene, exactly 2.93 Å at PBE-D2 level. When using PBE-D3 or PBE-D3BJ, this distance increases to 3.12 and 3.15 Å, respectively, although the change in

interaction energy is only reduced by 0.02 kJ mol^{-1} for PBE-D3, yet 0.41 kJ mol^{-1} for PBE-D3BJ. When using TS vdW correction, the H_2 is placed slightly farther away, at 3.20 Å, despite of the similar interaction energy of 5.51 kJ mol^{-1}.

Altogether, the diffusive nature of vdW interactions and the small differences among corrections do not allow connecting a farther adsorption distance to a smaller interaction energy. Indeed, such subtle differences are affected by the choice of the basis set, as using NAO or ANO imply a change of the interaction strength of up to 0.49 and 0.31 kJ mol^{-1}, respectively. In any case, one can claim that any of the employed corrections display an interaction energy of 5±1 kJ mol^{-1} which encompasses the CCSD(T) data at CBS limit,[66] and distances are also close to the reported value of 3.11 Å, with D3 and D3BJ only differing by 0.01 and 0.04 Å, respectively. Note that neglecting vdW leads to a weaker description of the interaction, with PBE values being 2 kJ mol^{-1} at most, with adsorption distances that can consequently reach distances of more than 4 Å, as observed in PBE calculations employing NAO basis set, in agreement with previous estimates.[65]

Table 1 Summary of PBE results, alone or combined with D2, D3, D3BJ, and TS vdW corrections, obtained using AIMS, VASP, or Gaussian code, on the interaction of H_2 over benzene in Pe, Pa_1, and Pa_2 conformations, see Fig. 1. Adsorption energies, E_{ads}, are given in kJ mol^{-1}, and H_2 bond lengths, *d*(HH), and the height of the H_2 molecular gravimetric center to the benzene plane, *h*, are given in Å. CCSD(T) values from literature are also provided.

Method	**Code**	**Site**	E_{ads} **/kJ mol^{-1}**	***d*(HH) /Å**	***h* /Å**
PBE	AIMS	Pe	1.42	0.75	4.12
	VASP	Pe	1.99	0.75	3.30
		Pa_1	0.89	0.75	3.30
		Pa_2	0.75	0.75	3.19
PBE-D2	Gaussian	Pe	5.79	0.75	2.96
	VASP	Pe	5.50	0.75	2.93
		Pa_1	3.95	0.75	2.83

		Pa_2	3.98	0.75	2.85
PBE-D3	Gaussian	Pe	5.79	0.75	3.13
	VASP	Pe	5.48	0.75	3.12
		Pa_1	4.38	0.75	2.99
		Pa_2	4.41	0.75	3.01
PBE-D3BJ	Gaussian	Pe	4.82	0.75	3.14
	VASP	Pe	5.09	0.75	3.15
		Pa_1	3.89	0.75	2.98
		Pa_2	3.88	0.75	2.97
PBE-TS	AIMS	Pe	6.02	0.75	3.26
	VASP	Pe	5.51	0.75	3.20
		Pa_1	4.63	0.75	2.97
		Pa_2	4.63	0.75	2.96
CCSD(T)		Pe[a]	3.06	—	—
		Pe[b]	4.34	0.74	3.11
		Pa_1[b]	3.06	0.74	3.06

[a] Ref. [68], [b] Ref. [66].

3.2. H_2 Adsorption on Graphene

Here we evaluate the H_2 interaction with graphene. To this end different high-symmetry adsorption sites are studied, including perpendicular positions over hexagonal rings of graphene (Pe_1), but also on top of a C atom (Pe_2), and bridging two C atoms (Pe_3), and parallel positions with H_2 bond pointing to C-C bonds (Pa_1), to opposite C atoms (Pa_2), over a C-C bond with H atoms pointing to the bond C atoms (Pa_3), perpendicular to Pe_3 (Pa_4), and on top of a C atom (Pa_5), see depictions in Fig. 2. The adsorption energies for each site are shown in Table 2 for each computational level under inspection.

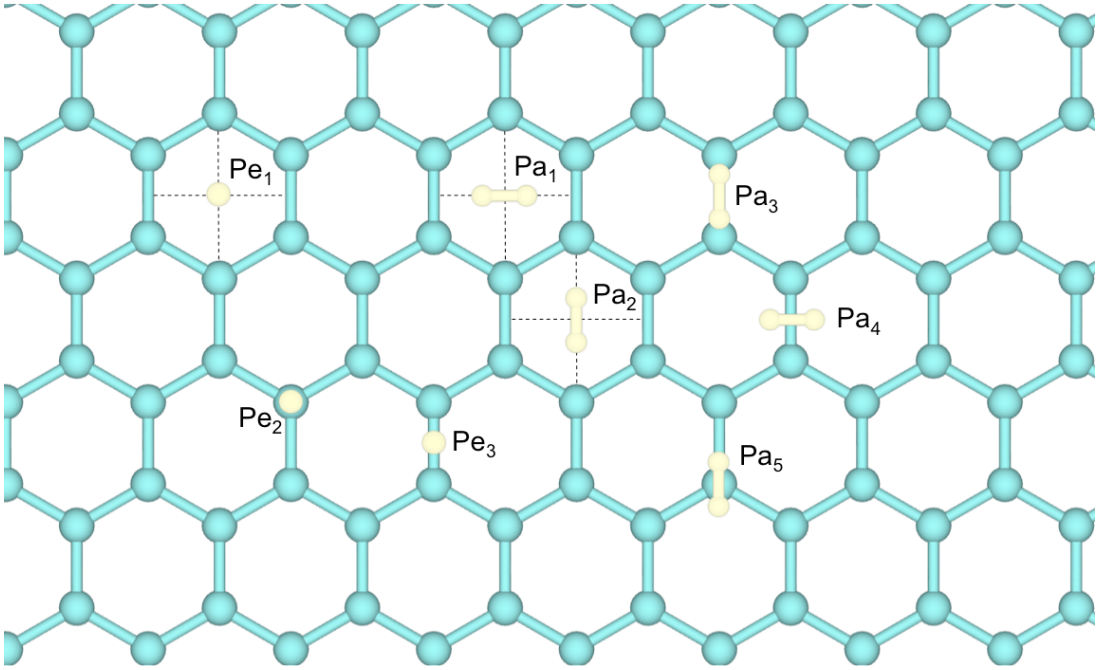

Fig. 2 Schematic representation of the adsorption sites of H_2 on graphene. Colouring code as in Fig. 1. Dashed lines guide the eye on the hexagonal rings of graphene.

A comparison can be made with respect CCSD(T) CBS limit calculations,[66] which showed a preference for Pe_1 with an E_{ads} of 5.44 kJ mol^{-1}, although Pa_1 was found to be essentially isoenergetic, with an E_{ads} of 5.43 kJ mol^{-1}. Present results at any level show a very similar adsorption strength at any site, with differences among sites spreading over 1.38 kJ mol^{-1} using D2, and reduced to 0.7 and 0.77 kJ mol^{-1} at D3 and D3BJ levels, so, close to the above-commented setup accuracy limit. The results over graphene are similar to the benzene situation, with an overestimation of 1-2 kJ mol^{-1} with respect CCSD(T) values. Here a direct comparison can be made with the experimentally determined adsorption energy of 5.00±0.05 kJ mol^{-1} from H_2 adsorption on graphite,[64] showing that the presently studied vdW corrections are slightly overestimating the adsorption strength by 1.4-2.2 kJ mol^{-1}, which we note as a measure of caution for the posterior interaction weighting.

Table 2 Summary of PBE results, alone or combined with D2, D3, D3BJ, and TS vdW corrections, on the interaction of H_2 over graphene conformations depicted in Fig. 2. Adsorption energies, E_{ads}, are given in kJ mol^{-1}.

E_{ads} / kJ mol^{-1}	PBE	PBE-D2	PBE-D3	PBE-D3BJ	PBE-TS
Pe_1	1.24	6.41	7.04	6.50	7.73
Pe_2	1.13	5.84	6.82	6.26	7.13
Pe_3	1.14	5.91	7.15	6.57	7.76
Pa_1	1.40	5.73	7.06	6.36	7.71
Pa_2	1.11	6.16	7.26	6.64	8.27
Pa_3	1.09	5.19	6.69	5.99	7.16
Pa_4	0.87	5.03	6.56	5.87	7.04
Pa_5	0.92	5.04	6.58	5.89	7.04

3.3. Transition Metal Adsorption on Graphene

As a last test, we compared the performance of D2, D3, D3BJ, and TS corrections on describing the interaction of the *full* sets of 3*d*, 4*d*, and 5*d* transition metal adatoms adsorbed on graphene, with the exception of La and Os in TS, because of the lack of atomic references and concomitant technical limitations. To this end, most stable sites as obtained in a previous study at PBE and PBE-D2 levels[29] have been optimized at PBE combined with D3, D3BJ, and TS, and the adsorption energies calculated. The transition metal adatoms are found to preferentially adsorb on the graphene hexagonal rings, except for Cr, Mo, Ag, W, and Pt, which prefer to bridge two neighbouring C atoms, Mn, Cu, Cd, Re, and Au, which prefer to sit atop of a C atom, and Ir, which adsorbs over the hexagonal ring, but slightly displaced to a neighbouring C atom. The E_{ads} trends along *d* series are shown in Fig. 3, whereas full sets of values are encompassed in Table S1 of Supporting Information. From the plots, one clearly observes that overall trends are captured using any of the vdW corrections under inspection, with mean absolute changes in E_{ads} of ~0.17 eV when using one or another correction. Only slight deviations from the general trend, for instance, for TS on Nb, where the E_{ads} is slightly

larger compared to other corrections, Ir TS, which is slightly smaller, or La D3BJ, which is slightly smaller —maybe due to the *f* electrons effect— as well, are found.

At this stage it seems that there is no strong arguments in selecting one or another vdW correction in describing neither the interaction of H_2 to benzene or graphene nor the attachment of TMs on graphene, as they overall describe the very same situation, although H_2 interaction may be overestimated by 1-2 kJ mol^{-1} when we regard the comparison in between H_2 attachment to graphene to that of graphite and the computational setup intrinsic precision. To this end, given the high accuracy of any of the methods, D3 correction has been chosen simply because there exist reports in the literature where its suitability is also highlighted for the interaction of H_2 with coronene and metal oxide clusters,[53,67] and shows no trends deviations.

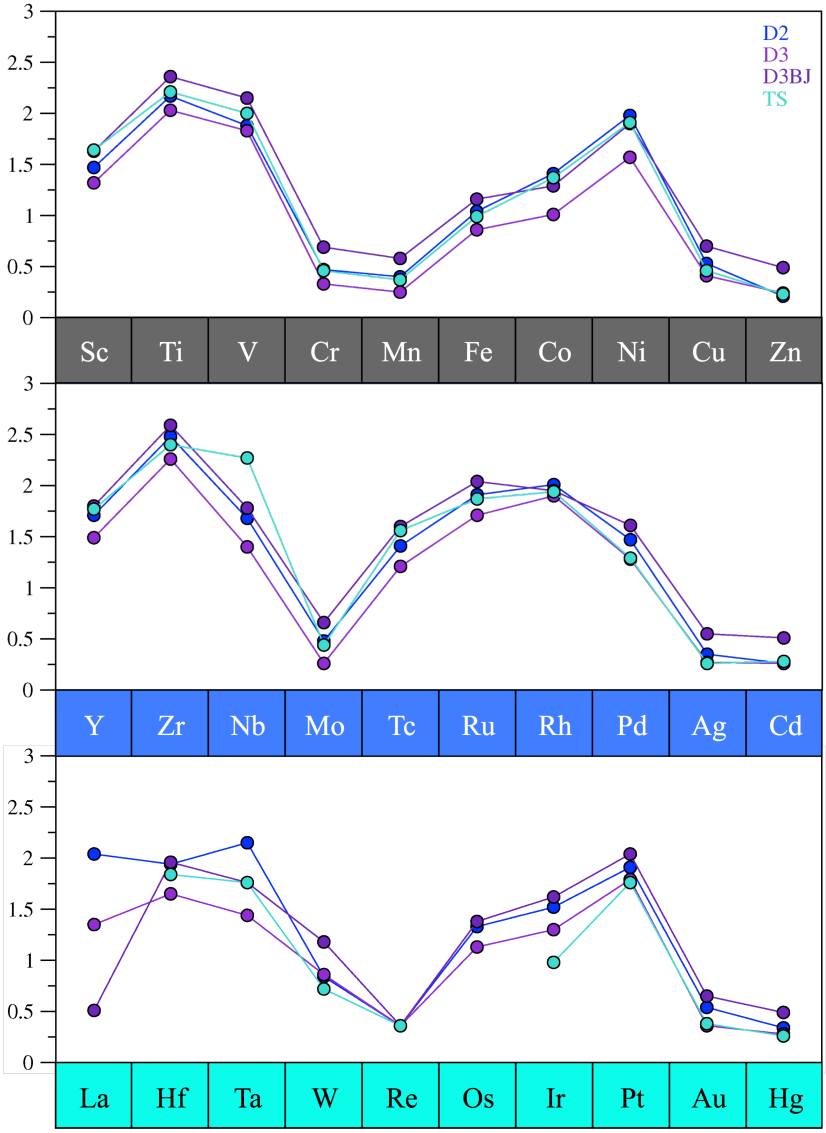

Fig. 3 Trends along the 3*d* (upper panel), 4*d* (middle panel), and 5*d* (bottom panel) series for the adsorption of the transition metal adatoms on graphene on most stable sites as depicted previously,[29] and plotted as calculated at PBE level using D2, D3, D3BJ, or TS methods to describe vdW forces.

3.4. Anchoring of H_2 to TMs/Graphene

Given that PBE-D3 is chosen as a highly-accurate computing level to describe the interaction of H_2 to benzene, graphene, and of transition metal adatoms to graphene, we inspect then at

this level and in a thorough manner the interaction of H_2 to the TM adatoms anchored to graphene. As above stated the TMs adsorb on graphene on the hexagonal rings, atop of C atoms, bridging two C atoms of a C-C bond, or in a displaced hexagonal ring for Ir case.[29] For these four types of TM adatoms several contact modes of H_2 adsorption have been explored, placing the H_2 molecule centre of mass 2 Å away from the metal adatom, and sampling different orientations, either flat and on top of the metal adatom (see example **a** in Fig. 4), in a leant position where one of the H atoms points to the graphene sheet and one to the metal adatom (see example **c** in Fig. 4), or flat over the graphene layer but coordinating as well to the metal adatom (see example **e** in Fig. 4). For each transition metal adatom typically two different orientations of the H_2 molecule with respect the graphene sheet have been sampled.

The optimization of the structures depicted in Fig. 4 at PBE-D3 level led, in most cases, to a collapse of the different explored configurations towards just one or two existing minima per TM, see exemplary final situations in Fig. 5. Aside, according to very different E_{ads} values and structural geometries, three markedly different final situations are depicted; either *i)* physisorbed H_2, in which the non-dissociated molecule remains essentially intact, with H_2 bond elongations below 0.06 Å and E_{ads} values below ~20 kJ mol^{-1}, *ii)* the so-called Kubas η^2 mode with the H_2 bond lengths elongated by ~0.06-0.16 Å and featuring increased E_{ads} values ranging 20-40 kJ mol^{-1},[16,17] and *iii)* a fully dissociated situation, where H atoms are placed well apart, typically involving large E_{ads} values and *d*(HH) distances. Kubas mode is labelled up to a profitable E_{ads} value of 60 kJ mol^{-1}.

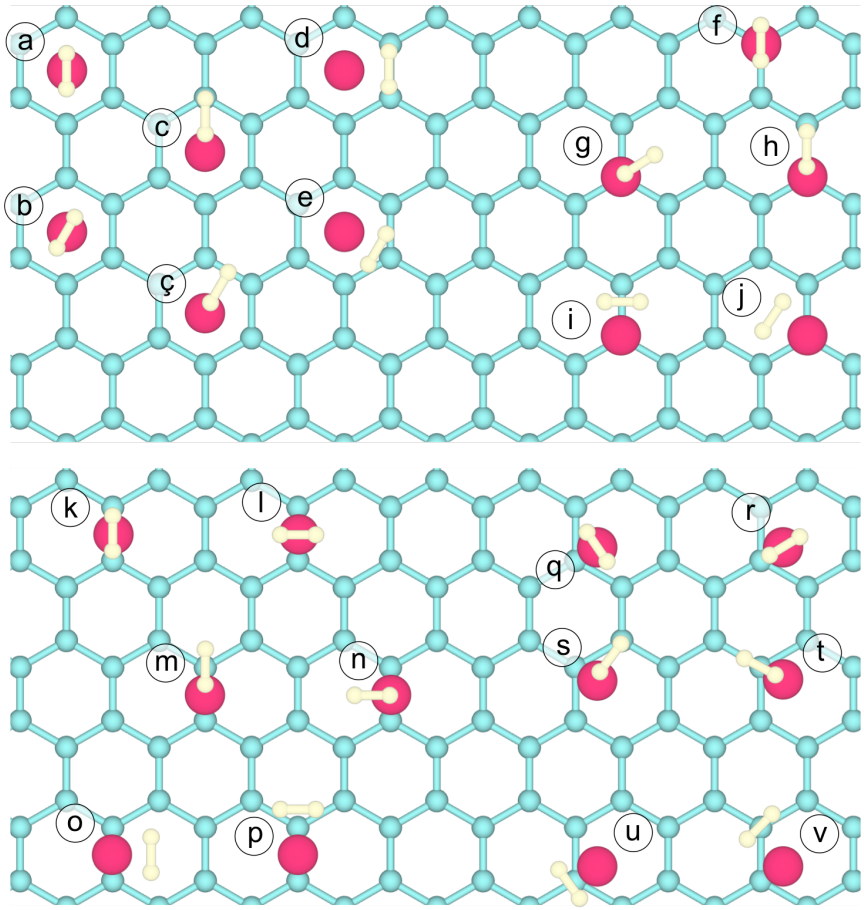

Fig. 4 Top view of the sites explored for H_2 adsorption over a transition metal adatom attached to graphene, either on a graphene hexagonal ring (**a**-**e**), a top of a C (**f**-**j**), over a C-C bridge (**k**-**p**), or displaced over the hexagonal ring (**q**-**v**). Colouring code as in Fig. 1, but with metal adatoms represented by a red sphere.

Table 3 summarizes the results of the most stable sites found for each explored TM, together with a notation on their physisorbed (**P**), Kubas (**K**), or dissociated (**D**) modes. Having a look at the different obtained modes of interaction, P situations typically imply a *d*(HH) of 0.75 Å, same as for the isolated H_2 molecule, or elongated by 0.02 Å at most, see exemplary case of Os in Fig. 5, whereas D situations place H atoms well apart, typically more than 1.8 Å, see *e.g.* case of La in Fig. 5. As above stated, the overall elongation of *d*(HH) for K modes ranges 0.06-0.16 Å. However, there are exceptions to these trends. For instance, a few 3*d* and 4*d* TM

cases, in particular, V, Co, Ni, Ru, Rh, and Pd feature relatively high E_{ads} values, above 70 kJ mol^{-1}, while H atoms are not fully dissociated, being located up to 1 Å apart, see Fig. 5. These cases are denoted as elongated Kubas (**K'**). The last singular case is Cr, where a dissociated situation is found, with a *d*(HH) of 2.39 Å, see Fig. 5, despite the E_{ads} falls within the Kubas energy range. However, given that H atoms are located well apart, it is denoted as dissociated. This dissociated situation is accompanied by a separation of circa 0.91 Å of Cr with respect the graphene sheet, in accordance with previous observations, and the concomitant higher activity.[30]

In order to explain the coordination mode preference, we recall the molecular orbital considerations available in the literature,[30] the chemical interaction of the TM with benzene showed the important interplay of $1a_1$ and $1b_1$ molecular orbitals, so that when going from dissociated to Kubas, these $1b_1$ orbitals featured a significant change in energy, associated to its shape, where the TM *d* predominant character affects the Kubas, and supremacy is for H_2 antibonding σ_u^* state in the case of dissociation. In the course of σ_u^* and d interaction, the H_2 bond lengthening gets more acute so far the *d* orbitals are more diffuse, and therefore, more overlap exists, and so, its influence is higher left on the series and down the groups, in perfect agreement with the here observed trends, with the caveats for physisorbed situations.

Thus, when plotting the E_{ads} values along the *d* series, Fig. 6, one immediately realizes that the list of TM could usable for H_2 storage is quite reduced; only Mn, Fe, and Zr; However, Sc, and Ti also feature a Kubas adsorption mode within the needed binding strength, see Supporting Information. These TMs are the most interesting ones as being the lightest TM explored, a point of interest in order to meet the gravimetric requirement, here, at the explored TM coverage, being of ~0.85% per H_2 molecule. However, their most stable situation is the dissociated one, although one has to notice that the H_2 bond (4.52 eV) should be broken from the precedent Kubas state, and present estimates of so, obtained by

successively enlarging the H_2 bond, place the energy barrier to be overcome above 60 kJ mol^{-1}; therefore, seems likely that H_2 would desorb rather than to dissociate, see Supporting Information.

Other appealing TMs are the scarce, precious metals of Ru, Rh, and Pd, and the more abundant V, Co and Ni. Despite their E_{ads} are larger than required, their Kubas mode, and the possibility of adsorbing a few H_2 molecules per TM adatom center, at the expense of reducing their interaction energy, tags them as interesting options to accumulate larger quantities of H_2 per center, although only one H_2 would adsorb on Ni when one would follow the 18 electrons counting rule.[30] Nonetheless, previous DF works showed the possibility of adsorbing in between 2 and 4 H_2 molecules per TM center (as found for 3*d* metals Sc, Ti, V, Cr, Mn, Fe, and Co) while meeting the adsorption energy criterion.[24,26,27,30] Thus, for instance, accounting for a double side occupancy of TMs and the possibility of attaching up to 4 H_2 per TM center, weight loads of 5.41 and 5.30 wt% could be achievable for Sc and Ti, respectively, while retaining Kubas H_2 adsorption.

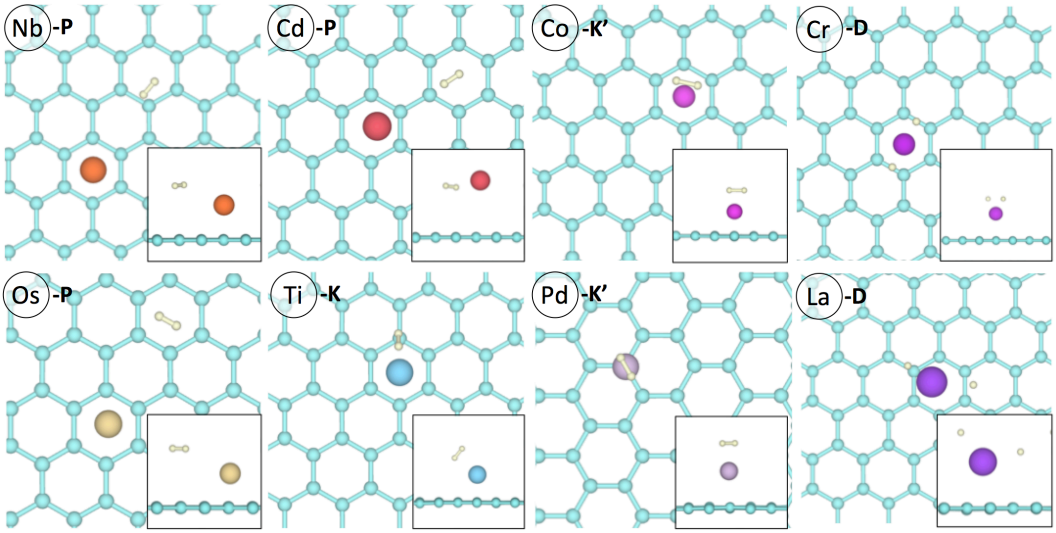

Fig. 5 Top (and side) views (in insets) for exemplary cases of H_2 in contact with diverse TM adatoms on graphene, alongside with their physisorbed (**P**), *Kubas* (**K**), elongated *Kubas* (**K'**),

and dissociated (**D**) situations. Colouring code as in Fig. 1, yet notice that metal adatoms are represented by differently coloured spheres.

Apart from that, Fig. 6 shows a clear differential behaviour in between 5*d* TMs, and 3*d* and 4*d* ones. The latter show a similar chemical activity among the series with few caveats, although 5*d* TMs clearly show an enhanced activity, with most of the transition metal adatoms dissociating H_2, strongly attaching the resulting H adatoms. These are presumably better suited when using these TMs on graphene as single-atom catalysts for hydrogenation reactions. Other than this, notice how the activity/reactivity follows the TM chemical (in)stability. Those transition metals featuring a semi or full occupancy of the *d* orbitals, i.e. the d^5 and d^{10} TMs, present a quite reduced interaction towards H_2 adsorption, being in all cases a physisorbed state.

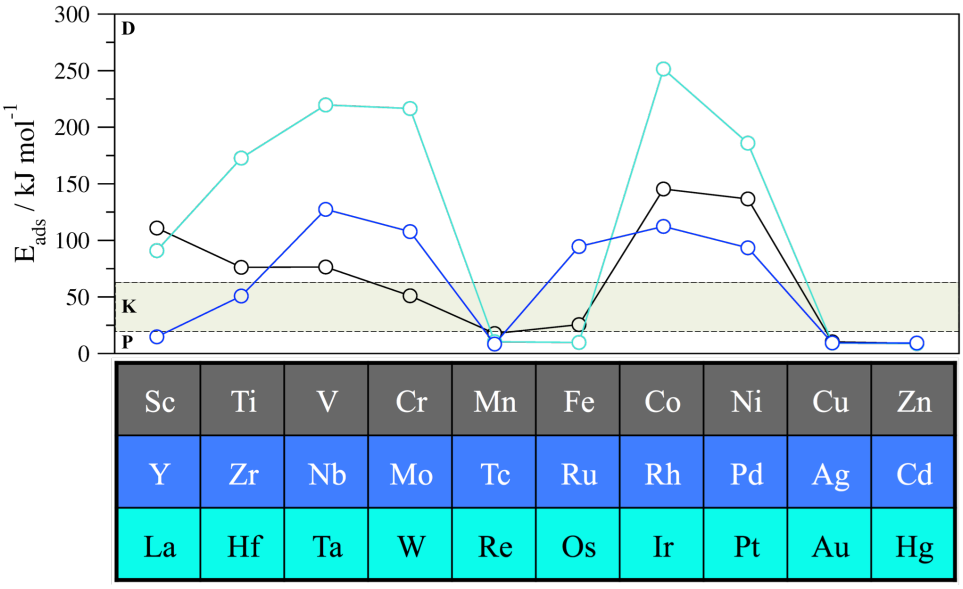

Fig. 6 Adsorption energies, E_{ads}, in kJ mol^{-1}, of H_2 in contact to full series of 3*d*, 4*d*, and 5*d* adatoms of TM@Graphene, with shaded regions showing physorbed (**P**), Kubas (**K**), and dissociated (**D**) modes. Colour code as *d* series in Fig. 3.

Table 3: Summary of PBE-D3 calculated results of H_2 adsorption on 3*d*, 4*d*, and 5*d* TM adsorbed on graphene, including the most stable adsorption mode, adsorption energy, E_{ads}, H_2 bond length, *d*(HH), mean H-TM bond length, $\bar{d}$(MH), overall H_2 Bader charge, Q_{H_2}, TM adatom net Bader charge, Q_{TM}, and total magnetic moment of the system, μ. Energies are in kJ mol^{-1}, distances in Å, Q in *e*, and μ in μ_B.

TM	Site	E_{ads} /kJ mol^{-1}	*d*(HH) /Å	$\bar{d}$(MH) /Å	Q_{H_2} /e	Q_{TM} /e	μ /μ_B
Sc	D	110.96	3.09	1.84	-1.14	1.70	0.00
Ti	D	76.22	3.06	1.76	-1.33	1.93	1.47
V	K’	76.53	0.83	1.89	-0.25	1.16	4.28
Cr	D	51.11	2.39	1.64	-1.05	1.33	3.98
Mn	P	17.72	0.76	3.67	-0.02	0.02	5.04
Fe	K	25.59	0.88	1.68	-0.14	0.74	0.50
Co	K’	145.55	0.95	1.56	-0.11	0.59	1.01
Ni	K’	136.63	0.91	1.54	-0.10	0.51	0.00
Cu	P	10.35	0.76	3.13	-0.02	0.16	0.99
Zn	P	8.96	0.75	3.48	-0.02	0.04	0.00
Y	K	14.75	0.82	2.24	-0.21	1.21	2.03
Zr	K	50.87	0.83	2.09	-0.30	1.71	2.52
Nb	D	127.39	2.10	1.78	-0.82	1.52	1.02
Mo	D	107.80	2.54	1.74	-1.17	1.61	3.65
Tc	P	8.39	0.75	3.79	-0.02	0.20	4.90
Ru	K’	94.54	0.89	1.76	-0.15	0.67	2.02
Rh	K’	112.38	1.00	1.86	-0.12	0.42	1.00
Pd	K’	93.47	0.87	1.71	-0.06	0.21	0.00
Ag	P	9.38	0.75	3.44	-0.02	0.04	1.00
Cd	P	9.28	0.75	3.74	-0.01	0.04	0.00
La	D	90.94	3.47	2.10	-1.17	1.82	0.00
Hf	D	172.71	3.00	1.87	-1.81	2.86	1.04
Ta	D	219.71	2.70	1.79	-1.76	2.92	1.01
W	D	216.55	2.68	1.74	-1.66	2.54	2.03
Re	P	10.44	0.75	3.71	-0.03	0.05	5.00
Os	P	9.84	0.75	4.79	0.00	0.60	2.03
Ir	D	251.46	2.00	1.59	-0.26	0.57	1.00
Pt	D	185.94	1.83	1.55	-0.26	0.27	0.00
Au	P	9.30	0.77	2.69	-0.02	0.07	0.92
Hg	P	8.81	0.75	3.47	-0.02	0.02	0.00

Furthermore, a double hump trend is observed in the case 5*d* TMs, in accordance to the *d* orbitals occupancy, as observed also for TM attachment on graphene, see Fig. 3.[29] The right hump is noticeable on 3*d* and 4*d* metals, yet quite hindered on early TMs. This goes along with the above commented preference of K situations left a series and up a group. Note that present estimates agree well with previous results of H_2 adsorption on 3*d* metal adatoms, as obtained at GGA level using the PW91 xc functional, where E_{ads} of 103.82, 77.48, 48.24, 116.27, and 133.44 kJ mol^{-1} were found for Sc, Ti, Cr, Co, and Ni, respectively, and so, within an energy window of 10 kJ mol^{-1}.[30] In addition, the dissociated state on Pt, with a E_{ads} of 185.94 kJ mol^{-1}, and a *d*(HH) of 1.83 Å, agrees well with that reported on Pt adatoms on CNTs of 113.85 kJ mol^{-1} and 1.86 Å, with differences mostly stemming from the curved nature of C network in CNTs;[31] indeed, the discrepancy is quite reduced when comparing to the Pt adatom adsorbed on a flat graphite (0001) surface, with an E_{ads} of 140.87 kJ mol^{-1}, and an exact *d*(HH) distance of 1.83 Å.

Structurally, it is worth highlighting that the H_2 bond length remains essentially 0.75 Å for physisorbed situations, and just slightly elongated for Kubas modes, to a maximum of 0.25 Å in K' Rh case. Only for the cases of dissociation, the H atoms are placed well apart, more than 1.7 Å distant, as shown in Fig. 7, and following the E_{ads} trend shown in Fig. 6. Concerning mean metal⟷hydrogen distance, $\bar{d}$(MH), Fig. 7 shows that for dissociated situations, such as on d^4 TMs Cr and Mo, and W, 3*d* Sc and Ti, and other 5*d* metals La, Hf, Ta, Ir, and Pt, the value is typically below 2 Å (2.1 Å in the case of La), in relation to the strong metal↔H adatom bond once H_2 is dissociated. In the case of elongated Kubas, the $\bar{d}$(MH) is below 1.9 Å, again reflecting the higher stage of H_2 elongation and the stronger bonding towards the TM centre, see Fig. 5.

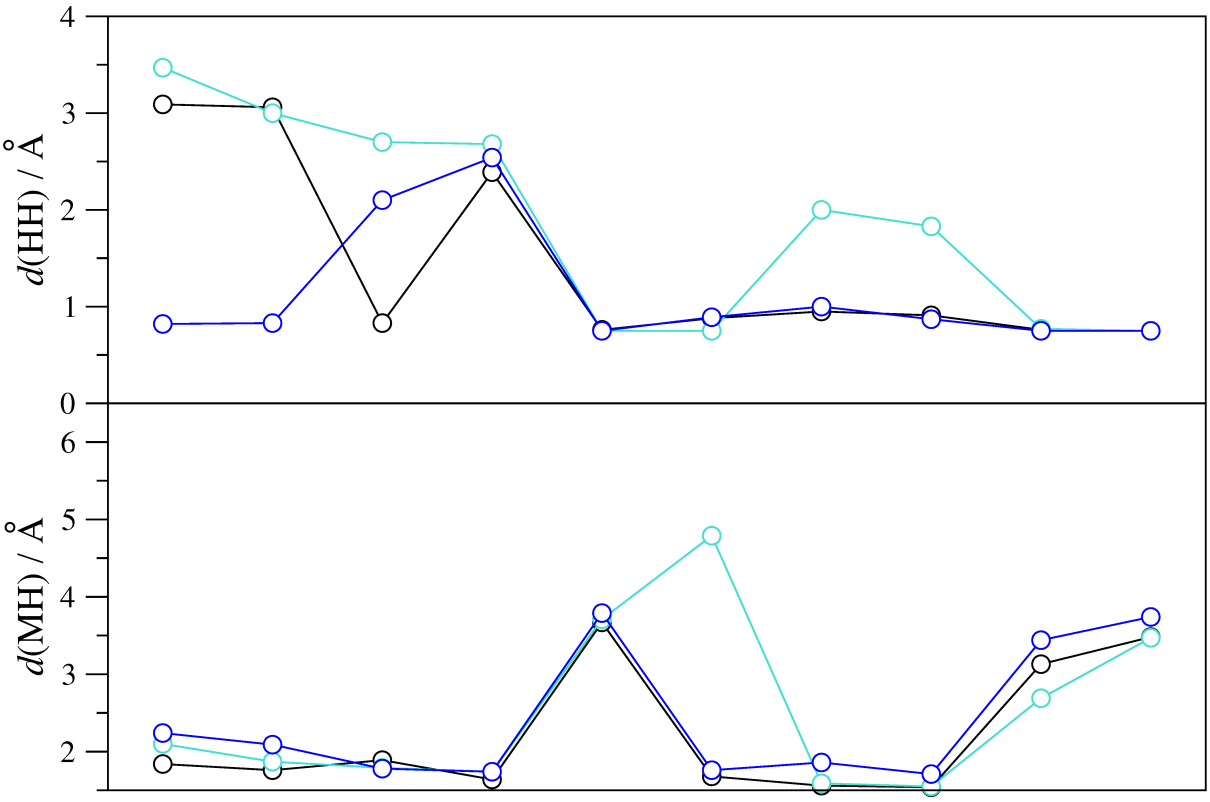

Fig. 7 H_2 bond lengths, *d*(HH), and mean H-TM distances, *d*(MH), both in Å, for H_2 adsorbed on most stable site on 3*d*, 4*d*, and 5*d* TM adatoms on graphene. Colour code as in Fig. 6.

As far as the electronic structure is concerned, Fig. 8 shows the Bader charges for TM adatoms and H_2 moieties. In all cases TMs feature positive charges (cations) whereas H_2 molecule, or H adatoms, present negative charges. Two clear trends are observed concerning this issue; *i)* the *d* TMs from d^5 and beyond feature substantially reduced charges compared to d^4 and before TMs, a fact somewhat observed before on a set of 3*d* TMs on graphene.[30] This implies a significant charge transfer from the TM@graphene systems towards the H_2 molecule, which somewhat goes along the adsorption strength as observed in Fig. 6, with a slight favourable preference on early *d* metals, and *ii)* the positive TM charge is mirrored, to a large extent, by the H_2 negative charge; so, the charge transfer is TM related, and the coulombic attraction between $TM^{\delta+}$ and $H_2^{\delta-}$ clear. In the case of Sc, Ti, La, Hf, Ta, W, Cr,

Nb, and Mo, the dissociated H adatoms can be safely catalogued as hydrides, with negative charges on H atoms ranging from -0.5 to -1 *e*.

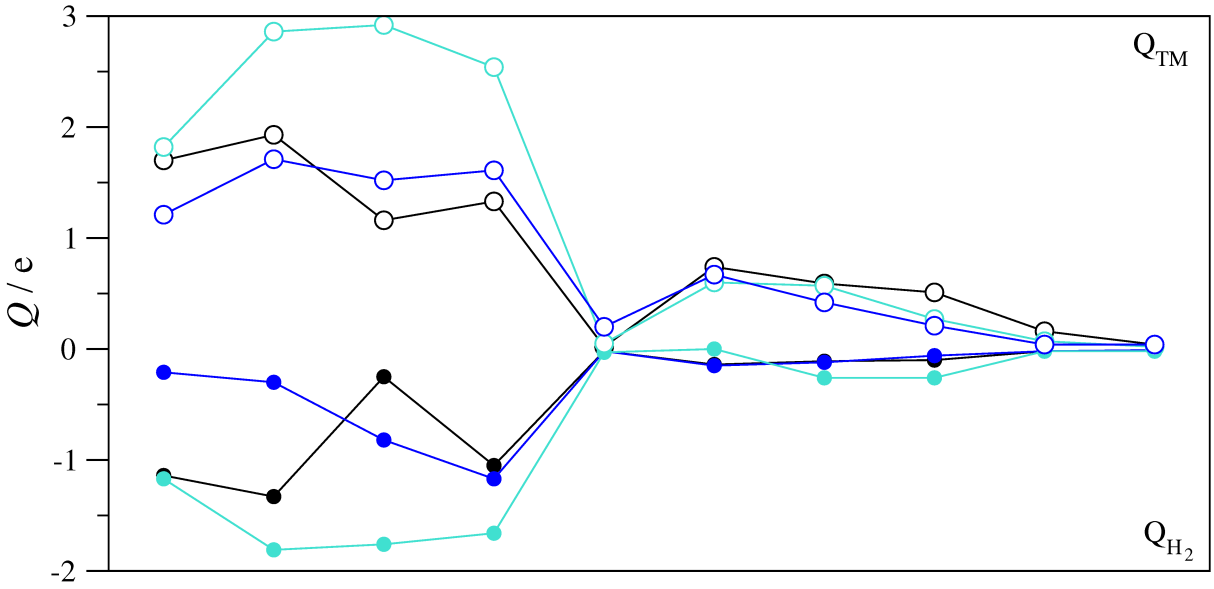

Fig. 8: Bader charges of H_2, Q_{H_2}– filled circles, and TM adatoms, Q_{TM} – open circles, adsorbed on graphene, both in *e*. Colour code as in Fig. 6.

Finally, magnetic features are plotted in Fig. 9, where the magnetization overall follows the observed trends of TM adatoms on graphene,[29] with the most significant differences being that at PBE-D3 level, late TMs such as Ir shows a magnetization of 1.00 μ_B, and Tc a value of 3.65 μ_B, where previous reported values at PBE-D2 with no H_2 adsorbed where of 0.06 and 0.56 μ_B, respectively. Further than that, early TMs, and specially 5*d* ones, reduce their magnetization by 2-3 μ_B compared to pristine TM@graphene situations, in clear accordance to the TM→H_2 charge transfer, H_2 dissociation, and hydride formation.

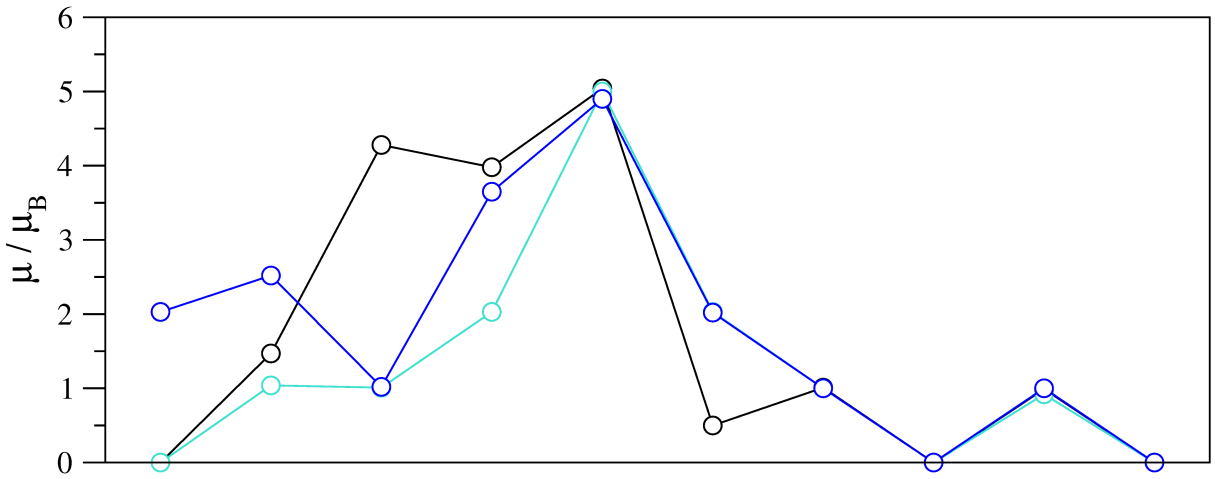

Fig. 9 Overall magnetization, μ, in μ_B, for H_2 adsorbed on most preferred situation on full sets of 3*d*, 4*d*, and 5*d* TM adatoms on graphene. Colour code as in Fig. 6.

In summary, the through investigation at DF PBE-D3 level of H_2 adsorption on *d* TMs attached on graphene reveals that the H_2 adsorption energy is quite low on those specially stable TMs with d^5 or d^{10} configuration. Aside, 5*d* metals, some of the leftmost 3*d* and 4*d* metals tend to dissociate H_2, and a significant share of TMs, Mn, Fe, Zr, V, Co, Ni, Ru, Rh, and Pd feature Kubas or elongated Kubas modes, where H_2 bond length is sensibly elongated, together with a H_2 binding strength enough to meet the energetic criterion for H_2 storage. The Sc and Ti cases feature also a Kubas mode which is appealing given the metal lightness, allowing, in ideal conditions, to meet the gravimetric condition, although other heavier metals may attach many H_2 moieties, given their higher interaction strength. The H_2 interaction with the TM adatom implies always a TM→H_2 charge transfer, where the positively charge on the TM cationic species is mostly counteracted by a negatively charge H_2 entity. Despite this, the magnetic moment of the system, stemming mostly from the TM adatom, is kept, except for early 5*d* TMs, where the unpaired electron transfer seems to be associated to the H_2 bond breakage.

4. Conclusions

Here we studied, in a thorough manner by means of DFT calculations employing vdW corrections, the interaction of H_2 to TM adatoms supported on graphene. Exploratory calculations comparing to CCSD(T) or experimental values reference data on the interaction of H_2 to benzene and graphene show that any of the vdW corrections under study, D2, D3, D3BJ, and TS, applied on PBE exchange-correlation functional, are similarly accurate to describe such subtle interactions. Moreover, the attachment strength of the *d* TMs on graphene is also reproduced by any of the methods. Thus, systematic adsorption interactions of H_2 in many contact manners to the TM adatoms is carried out at PBE-D3 level, revealing that H_2 just gets physisorbed on specially stable TMs with d^5 or d^{10} configuration. In the case of other 5*d* metals, and leftmost 3*d* and 4*d* metals, the H_2 molecule tends to dissociate, but a significant number of TMs (Mn, Fe, Zr, V, Co, Ni, Ru, Rh, and Pd) attach H_2 in the so-called Kubas or elongated Kubas modes, where H_2 bond length is sensibly elongated, together with a H_2 binding strength enough to meet the energetic criterion seek for H_2 storage. Sc and Ti feature also a Kubas mode suited for H_2 storage given their lightness, allowing, in ideal conditions where H_2 is not allowed to dissociate, to meet the gravimetric condition, despite other metals could be well suited when adsorbing a larger number of H_2 molecules. The H_2 interaction with the TM adatom is not only vdW type, but implies a TM→H_2 charge transfer, where the positively charge on the TM cationic species is mirrored by a negatively charge H_2 entity. The magnetic moment of the system tends to remain intact, except for early 5*d* TMs, where the unpaired electron transfer seems to be associated to the H_2 bond breakage.

Acknowledgements

The research carried out at the Universitat de Barcelona has been supported by the Spanish MINECO/FEDER grant CTQ2015-64618-R, and, in part, by *Generalitat de Catalunya* (grants 2014SGR97 and XRQTC) and from NOMAD Center of Excellence project; the latter

project has received funding from the European Union Horizon 2020 research and innovation program under grant agreement No 676580. F.V. thanks the MINECO for his postdoctoral *Ramón y Cajal* (RyC) research contract (RYC-2012-10129), F.I. acknowledges additional support from the 2015 ICREA Academia Award for Excellence in University Research, and A.G. is thankful for the SFRH/BPD/89722/2012 grant, the UID/MULTI/00612/2015 grant and to Diputación de Gipuzkoa for current funding in the frame of *Gipuzkoa Fellows* program.

Notes and References

1 http://www1.eere.energy.gov/hydrogenandfuelcells/storage/current_technology.html.

2 S. K. Bhatia and A. L. Myers, *Langmuir* 2006, **22,** 1688.

3 M. P. Suh, H. J. Park, T. K. Prasad, D.-W. Lim, *Chem. Rev*. 2012, **112**, 782.

4 R. Ströbel, J. Garche, P. T. Moseley, L. Jörissen, G. Wolf, *J. Power Sources* 2006, **159,** 781.

5 G. K. Dimitrakakis, E. Tylianakis, G. E. Froudakis, *Nano Lett.* 2008, **8**, 3166.

6 J. S. Arellano, L. M. Molina, A. Rubio, M. J. López, J.A. Alonso, *J. Chem. Phys.* 2002, **117**, 2281.

7 J. S. Arellano, L. M. Molina, A. Rubio, J.A. Alonso, *J. Chem. Phys.* 2000, **112**, 8114.

8 Y.-H. Kim, Y. Zhao, A. Williamson, M. J. Heben, S. B. Zhang *Phys. Rev. Lett.* 2006, **96**, 016102.

9 E. M. Kumar, S. Sinthika, R. Thapa, *J. Mater. Chem. A* 2015, **3**, 304.

10 Z. Zhou, J. Zhao, Z. Chen, X. Gao, T. Yan, B. Wen, P.v.R. Schleyer, *J. Phys. Chem. B* 2006, **110**, 13363.

11 I. Cabria, M. J. López, J. A. Alonso, *J. Chem. Phys.* 2005, **123**, 204721.

12 W. Liu, Y. H. Zao, Y. Li, Q. Jiang, E .J. Lavernia, *J. Phys. Chem. C* 2009, **113**, 2028.

13 F. Shayeganfar and R. Shahsavari *Langmuir* 2016, **32**, 13313.

14 E. Beheshti, A. Nojeh, P. Servati, *Carbon* 2011, **49**, 1561.

15 M. Yoon, S. Yang, C. Hicke, E. Wang, D. Geohegan, Z. Zhang, *Phys. Rev. Lett.* 2008, **100**, 206806.

16 G. J. Kubas, R. R. Ryan, B. L. Swanson, P. J. Vergamini, H. J. Wasserman, *J. Am. Chem. Soc.* 1984, **106**, 451.

17 G. J. Kubas, *J. Organomet. Chem.* 2001, **635**, 37.

18 L.-J. Zhou, Z. F. Hou, L.-M. Wu, Y.-F. Zhang, *J. Phys. Chem. C* 2014, **118**, 28055.

19 J. P. Perdew and K. Burke, *Phys. Rev. Lett.* 1996, **77**, 3865.

20 K. A. Gschneidner, *Solid State Phys.* 1964, **16**, 275.

21 J. P. Perdew and Y. Wang *Phys. Rev. B* 1992, **45**, 13244.

22 Q. Sun, P. Jena, Q. Wang, M. Marquez, *J. Am. Chem. Soc.* 2006, **128**, 9741.

23 Y. Zhao, Y.-H. Kim, A. C. Dillon, M. J. Heben, S. B. Zhang, *Phys. Rev. Lett.* 2005, **94**, 155504.

24 T. Yildirim, J. Íñiguez, S. Ciraci, *Phys. Rev. B* 2005, **72**, 153403.

25 Q. Sun, Q. Wang, P. Jena, Y. Kawazoe, *J. Am. Chem. Soc.* 2005, **127**, 14582.

26 T. Yildirim and S. Ciraci, *Phys. Rev. Lett.* 2005, **94**, 175501.

27 E. Durgun, S. Ciraci, T. Yildirim, *Phys. Rev. B* 2008, **77**, 085405.

28 H. Valencia, A. Gil, G. Frapper, *J. Phys. Chem. C* 2010, **114**, 14141.

29 M. Manadé, F. Viñes, F. Illas, *Carbon* 2015, **95**, 525.

30 H. Valencia, A. Gil, G. Frapper, *J. Phys. Chem. C* 2015, **119**, 5506.

31 S. Dag, Y. Ozturk, S. Ciraci, T. Yildirim, *Phys. Rev. B* 2005, **72**, 155404.

32 Y. Zhang, N.W. Franklin, R.J. Chen, H. Dai, *J. Chem. Phys.* 2000, **331**, 35

33 V.B. Parambhath, R. Nagar, S. Ramaprabhu, *Langmuir* 2012, **28**, 7826.

34 K.M. Fair, X.Y. Cui, L. Li, C.C. Shieh, R.K. Zheng, Z.W. Liu, B. Delley, M.J. Ford, S. P. Ringer, C. Stampfl, *Phys. Rev. B* 2013, **87**, 014102

35 H. Chang, M. Saito, T. Nagai, Y. Liang, Y. Kawazoe, Z. Wang, H. Wu, K. Kimoto, Y. Ikuhara, *Sci. Rep.* 2014, **4**, 6037.

36 E. Rangel, E. Sansores, *Int. J. Hydrogen Energy* 2014, **39**, 6558.

37 L. Ma, J.-M. Zhang, K.-W. Xu, *Appl. Surf. Sci.* 2014, **292**, 921.

38 B. Qiao, A. Wang, X. Yang, L. F. Allard, Z. Jiang, Y. Cui, J. Liu, J. Li, T. Zhang, *Nat. Chem.* 2011, **3**, 634.

39 A. Bruix, Y. Lykhach, I. Matolínová, A. Neitzel, N. Tsud, M. Vorokhta, V. Stetsovych, K. Ševčíková, J. Mysliveček, R. Fiala, M. Václavů, K.C. Prince, S. Bruyère, V. Potin, F. Illas, V. Matolín, J. Libuda, K.M. Neyman, *Angew. Chem. Int. Ed.* 2014, **53**, 10525.

40 K. Takahashi, Y. Tanaka, *Dalton Trans.* 2016, **45**, 10497.

41 C. Draxl, F. Illas, M. Scheffler, *Nature* 2017, **548**, 523.

42 A. Jain, S. P. Ong, G. Hautier, W. Chen, W. D. Richards, S. Dacek, S. Cholia, D. Gunter, D. Skinner, G. Ceder, K. A. Persson, *APL Materials* 2013, **1**, 011002.

43 https://www.materialsproject.org

44 https://www.nomad-coe.eu

45 G. Kresse and J. Furthmüller, *Phys. Rev. B* 1996, **54**, 11169.

46 P.E. Blöchl, *Phys. Rev. B* 1994, **50**, 17953.

47 P. Janthon, F. Viñes, S. M. Kozlov, J. Limtrakul, F. Illas, *J. Chem. Phys.* 2013, **138**, 244701.

48 P. Janthon, S. M. Kozlov, F. Viñes, J. Limtrakul, F. Illas, *J. Chem. Theory Comput.* 2013, **9**, 1631.

49 P. Janthon, S. J. Luo, S. M. Kozlov, F. Viñes, J. Limtrakul, D.G. Truhlar, F. Illas, *J. Chem. Theory Comput.* 2014, **10**, 3832.

50 H. J. Monkhorst and J. D. Pack, *Phys. Rev. B* 1976, **13**, 5188.

51 R. F. Bader, *Atoms in Molecules: A Quantum Theory*, Oxford Science, Oxford, U.K. 1990.

52 S. Grimme, J. Antony, S. Ehrlich, S. Krieg, *J. Chem. Phys.* 2010, **132**, 154104.

53 J. Gebhardt, F. Viñes, P. Bleiziffer, W. Hieringer, A. Görling, *Phys. Chem. Chem. Phys.* 2014, **16**, 5382.

54 S. Grimme, *J. Comp. Chem.* 2006, **27**, 1787.

55 M. Amft, S. Lebègue, O. Eriksson, N.V. Skorodumova, *J. Phys.: Condens. Matter.* 2011, **23**, 395001.

56 S. Grimme, S. Ehrlich, L. Goerigk, *J. Comp. Chem.* 2011, **32**, 1456.

57 A. Tkatchenko and M. Scheffler, *Phys. Rev. Lett.* 2009, **102**, 073005.

58 V. Havu, V. Blum, P. Havu, M. Scheffler, *J. Comput. Phys.* 2009, **228**, 8367.

59 V. Blum, R. Gehrke, F. Hanke, P. Havu, V. Havu, X. Ren, K. Reuter, M. Scheffler, *Comput. Phys. Commun.* 2009, **180**, 2175.

60 F. Viñes and F. Illas, *J. Comput. Chem.* 2017, **38**, 523.

61 M. J. Frisch, G. W. Trucks, H. B. Schlegel, G. E. Scuseria, M. A. Robb, J. R. Cheeseman, G. Scalmani, V. Barone, B. Mennucci, G. A. Petersson, H. Nakatsuji, M. Caricato, X. Li, H. P. Hratchian, A. F. Izmaylov, J. Bloino, G. Zheng, J. L. Sonnenberg, M. Hada, M. Ehara, K. Toyota, R. Fukuda, J. Hasegawa, M. Ishida, T. Nakajima, T. Honda, O. Kitao, H. Nakai, T. Vreven, J. A. Jr. Montgomery, J. E. Peralta, F. Ogliaro, M. Bearpark, J. J. Heyd, E. Brothers, K. N. Kudin, V. N. Staroverov, R. Kobayashi, J.

Normand, K. Raghavachari, A. Rendell, J. C. Burant, S. S. Iyengar, J. Tomasi, M. Cossi, N. Rega, N. J. Millam, M. Klene, J. E. Knox, J. B. Cross, V. Bakken, C. Adamo, J. Jaramillo, R. Gomperts, R. E. Stratmann, O. Yazyev, A. J. Austin, R. Cammi, C. Pomelli, J. W. Ochtrerski, R. L. Martin, K. Morokuma, V. G. Zakrzewski, G. A. Voth, P. Salvador, J. J. Dannenberg, S. Dapprich, A. D. Daniels, O. Farkas, J. B. Foresan, J. V. Ortiz, J. Cioslowski, D. J. Fox, Gaussian 09, Gaussian, Inc.: Wallingford, CT, 2009.

62 J. Almlöf and P. R. Taylor, *J. Chem. Phys.* 1987, **86**, 4070.

63 C. M. Brown, T. Yildirim, D. A. Newmann, M. J. Heben, T. Gennett, A. C. Dillon, J. L. Alleman, J. E. Fischer, *Chem. Phys. Lett.* 2000, **329**, 311.

64 L. Mattera, F. Rosatelli, C. Salvo, T. Tommasini, U. Valbusa, G. Vidali, *Surf. Sci.* 1980, **93**, 515.

65 C. Díaz, *Theor. Chem. Acc.* 2015, **134**, 105.

66 M. Rubeš and O. Bludský, *ChemPhysChem* 2009, **10**, 1868.

67 M. Kocman, P. Jurečka, M. Dubecký, M. Otyepka, Y. Cho, K. S. Kim, *Phys. Chem. Chem. Phys.* 2015, **17**, 6423.

68 O. Hübner, A. Glöss, M. Fichtner, W. Klopper, *J. Phys. Chem. A* 2004, **108**, 3019.

69 M. Dion, H. Rydberg, E. Schröder, D. C. Langreth, B. I. Lundqvist, *Phys. Rev. Lett.* 2004, **92**, 246401.